Research Article | Vol. 25, No. 7 | 3 Apr 2017 | OPTICS EXPRESS 7999

Optics EXPRESS

Phase stability of photoreceivers in intersatellite laser interferometers

GERMÁN FERNÁNDEZ BARRANCO,[1,2,*] OLIVER GERBERDING,[1,2] THOMAS S. SCHWARZE,[1,2] BENJAMIN S. SHEARD,[1,2,3] CHRISTIAN DAHL,[1,2,4] BERND ZENDER,[5] AND GERHARD HEINZEL[1,2]

[1]*Max Planck Institute for Gravitational Physics (Albert Einstein Institute), Callinstrasse 38, 30167 Hanover, Germany*
[2]*Institut für Gravitationsphysik, Leibniz Universität Hannover, Callinstrasse 38, 30167 Hanover, Germany*
[3]*Currently with EOS Space Systems Pty Limited, EOS House Mount Stromlo Observatory, Bart Bok Road, Stromlo, ACT 2611, Australia*
[4]*Currently with SpaceTech GmbH (STI), Seelbachstrasse, 88090 Immenstaad am Bodensee, Germany*
[5]*German Aerospace Center (DLR), Rutherfordstrasse 2, 12489 Berlin, Germany*
[*]*German.Fernandez.Barranco@aei.mpg.de*

Abstract: A photoreceiver (PR) is required for the opto-electrical conversion of signals in intersatellite laser interferometers. Noise sources that originate or couple in the PR reduce the system carrier-to-noise-density, which is often represented by its phase noise density. In this work, we analyze the common noise sources in a PR used for space-based interferometry. Additionally, we present the results from the characterization of the PRs in GRACE-FO, a mission which will pioneer intersatellite laser interferometry. The estimated phase noise is shot-noise limited at 10^{-4} rad/Hz$^{1/2}$ down to 10^{-2} Hz, almost 4 orders of magnitude below the instrument top level requirement (0.5 rad/Hz$^{1/2}$). Below 10^{-2} Hz, the PR finite phase response noise dominates but the levels still comply with the instrument requirement. The sub-mHz noise levels and the PR electronic noise have been identified as key design factors for the LISA PR.

OCIS codes: (120.0120) Instrumentation, measurement, and metrology; (120.3180) Interferometry; (120.4640) Optical instruments; (060.2840) Heterodyne; (230.5170) Photodiodes.

References and links

1. A. Chaddad, "Low-noise front-end receiver dedicated to biomedical devices: NIRS acquisition system," Circuits Systems **5**, 191–200 (2014).
2. F. Guzmán Cervantes, J. Livas, R. Silverberg, E. Buchanan, and R. Stebbins, "Characterization of photoreceivers for LISA," Classical Quantum Gravity **28**, 094010 (2011).
3. O. Gerberding, "Phase readout for satellite interferometry," Ph.D. thesis, Leibniz Universität Hannover (2014).
4. O. Gerberding, C. Diekmann, J. Kullmann, M. Tröbs, I. Bykov, S. Barke, N. Brause, J. E. Delgado, T. S. Schwarze, J. Reiche, K. Danzmann, T. Rasmussen, T. Hansen, A. Enggaard, S. Pedersen, O. Jennrich, M. Suess, Z. Sodnik, and G. Heinzel, "Readout for intersatellite laser interferometry: Measuring low frequency phase fluctuations of high-frequency signals with microradian precision," Rev. Sci. Instrum. **86**, 074501 (2015).
5. B. S. Sheard, G. Heinzel, K. Danzmann, D. A. Shaddock, W. M. Klipstein, and W. M. Folkner, "Intersatellite laser ranging instrument for the GRACE follow-on mission," J. Geodesy. **86**, 1083–1095 (2012).
6. K. Case, G. Kruizinga, and S. Wu, *GRACE Level 1B Data Product User Handbook* (JPL, 2010).
7. A. Sutton, K. McKenzie, B. Ware, and D. A. Shaddock, "Laser ranging and communications for LISA," Opt. Express **18**, 20759–20773 (2010).
8. G. Fernández Barranco, M. Tröbs, V. Müller, O. Gerberding, F. Seifert, and G. Heinzel, "Spatially resolved photodiode response for simulating precise interferometers," Appl. Opt. **55**, 6688–6693 (2016).

1. Introduction

With laser interferometry we can measure length variations between satellites with ultra-high precision. This is the main technology behind the Laser Interferometer Space Antenna (LISA), the future space-based gravitational wave detector. Additionally, the Gravity Recovery and Climate Experiment Follow-On (GRACE-FO) mission, designed to continue gravity-field measurements

#282257 https://doi.org/10.1364/OE.25.007999
Journal © 2017 Received 19 Dec 2016; revised 7 Feb 2017; accepted 7 Feb 2017; published 29 Mar 2017

Optics EXPRESS

from its predecessor, will include a laser ranging interferometer (LRI) that will enhance the precision of the main microwave instrument. A laser interferometer requires the use of photoreceivers (PRs), devices that convert optical signals into adequate electrical signals for the subsequent readout stages. The conditions present in an intersatellite interferometry system set hard requirements on the PRs, particularly on their noise contribution since MHz optical beat notes with amplitudes of tens of pW need to be detected.

Previous literature on low noise PR for kHz applications [1] or LISA-like photoreceivers [2] focuses on the electronic noise at component-level for PRs that feature only the photodetector and the first amplification stage. In this work, we present a detailed system-level analysis of a PR designed for space-based interferometry. This type of PR contains additional electronic stages and is also susceptible to other application specific noise sources. The analysis includes the experimental characterization of the PRs used in GRACE-FO, a mission that will feature intersatellite laser interferometry for the first time.

In Section 2, we analyze the noise sources in the PR and show the noise budget derived from PR requirements and expected interferometer parameters in GRACE-FO. In Section 3, we provide a general overview of the GRACE-FO PR, including the photodetector and the pre-amplifier used. Section 4 contains a description of setups used to characterize the GRACE-FO PR and the results obtained. Finally, conclusions are provided in Sections 5.

2. Noise sources and PR requirements

Figure 1 shows a simplified block diagram of the PR stages within the interferometer metrology chain. The optical beat note, represented as a red sinusoid, arrives at the PR (dashed line). A photodetector, commonly a photodiode (PD), absorbs the photons of the incoming light and produces a current. This current is converted into voltage by the transimpedance amplifier (TIA). The signal at the output of the TIA passes through the anti-aliasing filter (AAF) to filter out high frequency signals and noise above the Nyquist frequency. In some designs, the AAF is not located in the PR but in the input of the following stage. For this work, we include the AAF in the PR since that is the configuration of the GRACE-FO PR and the baseline for future designs. Once the signal is filtered, it is transmitted from the output of the PR to the phasemeter (PM), where the signal is digitized and its phase measured. The actual implementation of a PR for intersatellite laser interferometry contains 4 times the structure just described since quadrant photodiodes (QPDs) are used instead of single-element photodiodes (SEPD) to measure angular misalignment between the interfering beams.

The carrier-to-noise-density of the system (C/N_0), common in satellite communications, can be used to analyze different noise contributions in a PR like the one in Fig. 1. However, the inverse of C/N_0 directly provides the noise spectral density of the metrology system in terms of phase [3]. This is because noise (e.g. amplitude fluctuations) at the optical beat note frequency is converted into phase noise by the phase measurement system, making it indistinguishable from the actual phase of the beat note. Since the phase of the beat note is the main measurand aimed at, working with phase noise densities is chosen for convenience. For simplification, our analysis focuses on a single channel of the PR. The beat note signal (carrier) has a root mean square value after photo-conversion given by:

$$i_{\mathrm{bn}} = R(2\gamma P_{\mathrm{LO}} P_{\mathrm{RX}})^{1/2} \quad [\mathrm{A}], \tag{1}$$

where R is the responsivity of the PD given in A/W, γ is the heterodyne efficiency of the interferometer and P_{LO} and P_{RX} are the optical powers of the two interfered beams on the PD surface. P_{LO} corresponds to the power of the local laser and P_{RX} to the power of the received beam from the distant spacecraft.

The first noise contribution presented is shot noise. Shot noise does not originate in the PR, but it is intrinsic to the photodetection process and used as reference level in noise budgets [3].

Optics EXPRESS

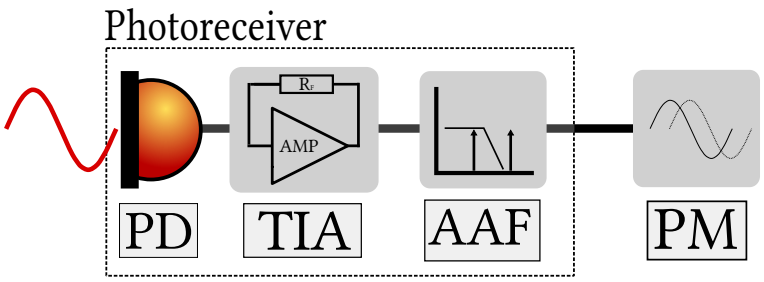

Fig. 1. Block diagram of the PR stages within the interferometer metrology chain. The optical beat note, represented as a red sinusoid, arrives at the PR (dashed line). A photodetector, commonly a photodiode (PD), absorbs the photons of the incoming light and produces a current. This current is converted into voltage by the transimpedance amplifier (TIA). The signal at the output of the TIA passes through an anti-aliasing filter (AAF) to filter out undesired signals and noise above the Nyquist frequency. Once the signal is filtered, it is transmitted from the output of the PR to the phasemeter (PM), where the signal is digitized and its phase measured.

The amplitude spectral density of shot noise is given by:

$$\tilde{\imath}_{\mathrm{sn}} = (2qR(P_{\mathrm{LO}} + P_{\mathrm{RX}}))^{1/2} \quad [\mathrm{A/Hz^{1/2}}], \tag{2}$$

with q being the charge of an electron. Symbols with tilde represent spectral densities. Now, we use the inverse of the C/N_0 to obtain the phase noise density contribution from shot noise:

$$\tilde{\phi}_{\mathrm{sn}} = \frac{\tilde{\imath}_{\mathrm{sn}}}{i_{\mathrm{bn}}} = \left(\frac{q(P_{\mathrm{LO}} + P_{\mathrm{RX}})}{R\gamma P_{\mathrm{LO}} P_{\mathrm{RX}}}\right)^{1/2} \quad [\mathrm{rad/Hz^{1/2}}]. \tag{3}$$

In a similar fashion, we can calculate the contribution of electronic noise (resistors Johnson-Nyquist noise, OpAmp noise...). This noise $\tilde{\imath}_{\mathrm{en}}$ is usually referred to the input of the PR and is given directly in $\mathrm{A/Hz^{1/2}}$. A detailed description of the electronic noise in a PR can be found in [2]. It is important to remark that $\tilde{\imath}_{\mathrm{en}}$ refers to electronic noise in the MHz band, which produces amplitude fluctuations at the beat note frequency. In the analysis, we do not take into account low frequency electronic noise from the phase measurement system or upconversion of low frequency PR electronic noise into the MHz band. The phase noise contribution from the PR electronic noise is:

$$\tilde{\phi}_{\mathrm{en}} = \frac{\tilde{\imath}_{\mathrm{en}}}{i_{\mathrm{bn}}} = \frac{\tilde{\imath}_{\mathrm{en}}}{R(2\gamma P_{\mathrm{LO}} P_{\mathrm{RX}})^{1/2}} \quad [\mathrm{rad/Hz^{1/2}}]. \tag{4}$$

The following noise sources are less common in the literature. A previous analysis of their effects on the PM can be found in [4]. The first one is the thermal-induced phase noise in the PR. Temperature variations in the spacecraft area where the PR is located produce changes in the phase response of the PR, inducing noise. The AAF is particularly susceptible to phase fluctuations over temperature due to its typically steep frequency response. Thanks to temperature simulations, we can anticipate the temperature stability in the satellite, a factor $\tilde{T}_{\mathrm{PR}}$ given in $\mathrm{K/Hz^{1/2}}$. The dependency of the main longitudinal phase ϕ_{L} over temperature could be measured experimentally, obtaining a coefficient ϕ_{LT} given in rad/K. This coefficient could in general be a function of the absolute temperature, but experimental results from PR characterization (Section 4) showed a mostly linear relationship between phase and temperature. This means that the coefficient is constant at least for the temperature range used. The thermal-induced phase noise contribution in the PR can then be obtained using:

Optics EXPRESS

$$\tilde{\phi}_{\mathrm{tin}} = \tilde{T}_{\mathrm{PR}}\phi_{\mathrm{LT}} \quad [\mathrm{rad/Hz^{1/2}}]. \tag{5}$$

The last noise source of this analysis comes from the finite phase response of the PR. Operating in the MHz range, the PR phase response over frequency is not flat, having a coefficient ϕ_{LF} given in rad/Hz. The coefficient ϕ_{LF} is frequency dependent, but in this analysis we use a constant, worst case value. Changes in the frequency of the beat note would couple as phase variations in the system. Lasers used in intersatellite interferometry present a frequency noise $\tilde{f}_{\mathrm{laser}}$, given in $\mathrm{Hz/Hz^{1/2}}$, which would appear as phase noise. Additionally, the dynamics of the beat note frequency due to relative spacecraft motion, with an amplitude spectral density $\tilde{f}_{\mathrm{Doppler}}$ given in $\mathrm{Hz/Hz^{1/2}}$, would also couple as phase variations via the finite phase response. This $\tilde{f}_{\mathrm{Doppler}}$ can be estimated from the spectral density of the relative velocity between the satellites [5]. Here we have used orbit data from the original GRACE mission to calculate $\tilde{f}_{\mathrm{Doppler}}$ [6]. Strictly speaking, this contribution from $\tilde{f}_{\mathrm{Doppler}}$ is not a purely stochastic component of the phase noise density, since it can be tracked and corrected in post-processing. Expression 6 shows the total contribution due to the finite phase response of the PR:

$$\phi_{\mathrm{fpn}} = (\tilde{f}^{\,2}_{\mathrm{laser}} + \tilde{f}^{\,2}_{\mathrm{Doppler}})^{1/2}\phi_{\mathrm{LF}} \quad [\mathrm{rad/Hz^{1/2}}]. \tag{6}$$

Figure 2 shows the phase noise budget for one PR channel obtained using the PR requirements and expected interferometer parameters for GRACE-FO (see Table 1). The red curve represents the total noise in the PR $\tilde{\phi}_{\mathrm{N}}$, using the incoherent sum of the noise sources described along Section 2. The PR is shot-noise limited at 10^{-4} $\mathrm{rad/Hz^{1/2}}$ down to 10^{-2} Hz, where the finite phase response noise begins to dominate due to its $\tilde{f}_{\mathrm{Doppler}}$ contribution. Two peaks are clearly visible at very low frequencies, corresponding to the orbital period of the satellites. The blue curve shows the top level noise requirement for the LRI $\tilde{\phi}_{\mathrm{LRI}}$, with a target frequency band between $2{\cdot}10^{-3}$ Hz and 10^{-1} Hz (solid line) [5]. This band was extended in Fig. 2 (dashed line) for comparison with the PR phase noise. The flat part of $\tilde{\phi}_{\mathrm{LRI}}$ corresponds to 80 $\mathrm{nm/Hz^{1/2}}$ of length precision, and it is dominated by laser noise and tilt-to-length coupling driven by pointing jitter [5]. In the shot-noise limited part, $\tilde{\phi}_{\mathrm{N}}$ is almost 4 orders of magnitude below $\tilde{\phi}_{\mathrm{LRI}}$. Additionally, the total noise $\tilde{\phi}_{\mathrm{N}}$ will improve when using the PR in hot redundancy (explained in Section 3) with all channels. The difference between $\tilde{\phi}_{\mathrm{N}}$ and $\tilde{\phi}_{\mathrm{LRI}}$ decreases towards low frequencies due to the influence of the finite phase response noise contribution. This noise level in the sub-mHz range complies with the extended top level requirement, but indicates that correction in post-processing might be chosen for further reduction of this noise contribution if necessary. This could also be a potential issue for the LISA mission and the LISA PR due to its more stringent noise budget [7]. On the other hand, $\tilde{f}_{\mathrm{Doppler}}$ effects in LISA are expected out-of-band (below 10^{-4} Hz).

Optics EXPRESS

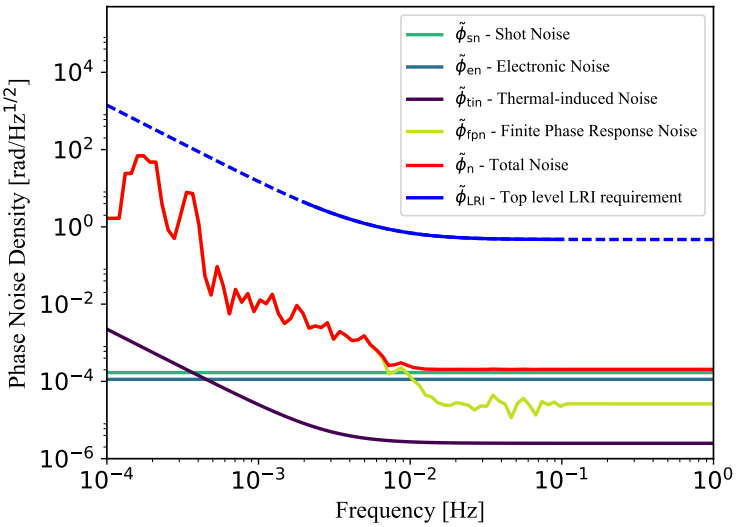

Fig. 2. Phase noise budget for one PR channel obtained using the PR requirements and expected interferometer parameters for GRACE-FO. The values used are summarized in Table 1. The red curve represents the total noise in the PR $\tilde{\phi}_{\mathrm{N}}$ from the noise sources described along Section 2. The PR is shot-noise limited at 10^{-4} rad/Hz$^{1/2}$ down to 10^{-2} Hz, where the finite phase response noise begins to dominate. The blue curve shows the top level noise requirement for the LRI $\tilde{\phi}_{\mathrm{LRI}}$, which needs to be fulfilled between $2{\cdot}10^{-3}$ Hz and 10^{-1} Hz (solid line) but was extended in this plot (dashed line) for comparison with the PR phase noise. In the shot-noise limited section, $\tilde{\phi}_{\mathrm{N}}$ is almost 4 orders of magnitude below $\tilde{\phi}_{\mathrm{LRI}}$. This margin decreases towards low frequencies due to the influence of the finite phase response noise contribution. This noise level in the sub-mHz range complies with the extended top level requirement, but indicates that post-processing correction might be chosen for further reduction of this noise contribution.

Table 1. PR requirements and expected interferometer parameters for GRACE-FO. Values with an asterisk (*) show only the noise floor at 1 Hz for simplification. In reality, they increase towards low frequencies as seen in Fig. 2. Based on the expected orbit dynamics in GRACE-FO, $\tilde{f}_{\mathrm{Doppler}}$ changes along the measurement band and therefore no specific value is given in this table. Experimentally measured values for $\tilde{\imath}_{\mathrm{en}}$ and ϕ_{LT} of the GRACE-FO PR flight model are given in Section 4.

P_{LO}	250	μW
P_{RX}	10	pW
R	0.7	A/W
γ	0.8	-
$\tilde{\imath}_{\mathrm{en}}$	5	pA/Hz$^{1/2}$
T_{PR}	10^{-4}*	K/Hz$^{1/2}$
ϕ_{LT}	$2.5 \cdot 10^{-2}$	rad/K
$\tilde{f}_{\mathrm{laser}}$	30*	Hz/Hz$^{1/2}$
ϕ_{LF}	$2 \cdot 10^{-7}$	rad/Hz

Optics EXPRESS

3. The GRACE-FO PR

The German Aerospace Center (DLR), in collaboration with the Max Planck Institute for Gravitational Physics, designed and built a set of PRs to fulfill the GRACE-FO mission requirements. The topology used is equivalent to the PR in Fig. 1. The FCIQ1000, a 1 mm diameter InGaAs QPD was chosen as photodetector. The spatially resolved profile of the FCIQ1000 was studied in [8]. An electrical diagram of the TIA can be seen in Fig. 3. The current from the reverse-biased photodiode (V_{bias} = 5 V) splits into an AC (main signal) and a DC path. Two OpAmp-based TIAs, featuring the LMH6624 (AC) and the OP284 (DC), convert the current into voltage (V_{AC}, V_{DC}).

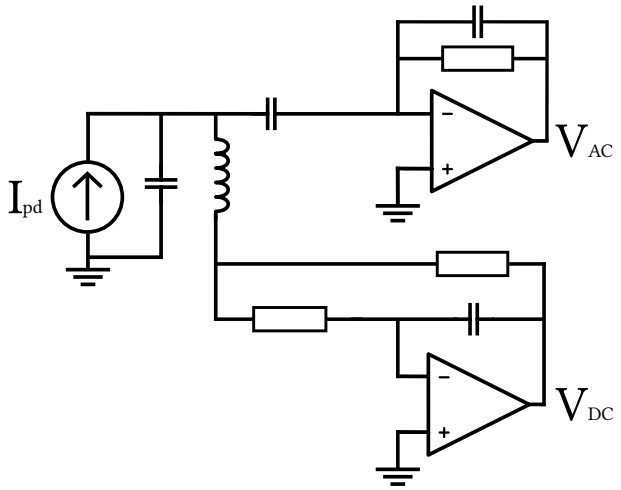

Fig. 3. Electrical diagram of the TIA from the GRACE-FO PR. The current from the reverse-biased photodiode (V_{bias} = 5 V) splits into an AC (main signal) and a DC path. Two OpAmp-based TIAs, featuring the LMH6624 (AC) and the OP284 (DC), convert the current into voltage (V_{AC}, V_{DC}).

The main difference between the GRACE-FO PR and the basic PR structure of Fig. 1 is the existence of two photoreceiver front-ends (PRFs) with independent PDs and TIAs sharing a common photoreceiver back-end (PRB), which includes a summing amplifier and the AAF. This topology is shown in Fig. 4. The two (identical) beat notes produced in the interferometer arrive at both PRFs and their output voltages are combined in the summing amplifier of the PRB prior to the AAF. The topology is essentially the same for the DC and the AC paths, differing in the OpAmp used for the summing amplifier (LT1498 for DC and AD8001 for AC). Hot redundancy operation is the nomenclature used when both PRFs are used at the same time.

Optics EXPRESS

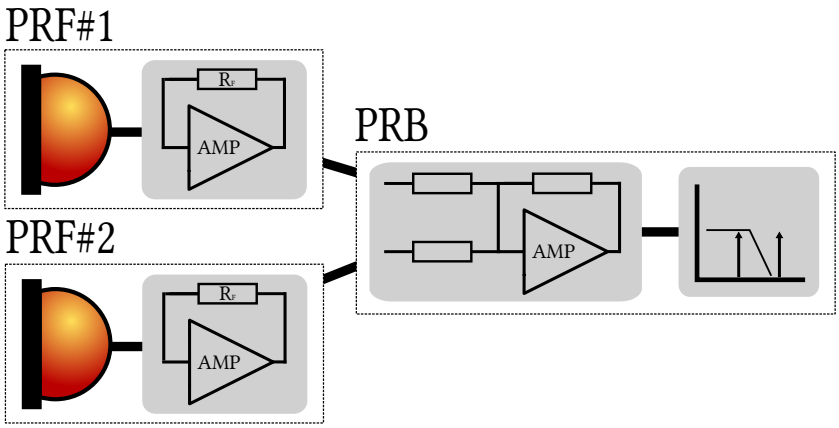

Fig. 4. Block diagram of the hot redundancy configuration: two photoreceiver front-ends (PRFs) with independent PDs and TIAs sharing a common photoreceiver back-end (PRB), which includes a summing amplifier and the AAF. The output voltages of the two PRFs are combined in the summing amplifier of the PRB prior to the AAF. The topology is essentially the same for the DC and the AC paths, differing in the OpAmp used for the summing amplifier (LT1498 for DC and AD8001 for AC).

4. Photoreceiver characterization

In this section, we present our efforts to experimentally measure the electronic noise contribution $\tilde{\imath}_{\mathrm{en}}$, the longitudinal phase temperature coefficient ϕ_{LT} and the differential phase temperature coefficient ϕ_{DiffT} (between QPD channels) of the GRACE-FO PR flight models. A simple measurement of the PR electronic noise $\tilde{\imath}_{\mathrm{en}}$ is possible with a shot-noise limited light source. This method does not require the use of the PR transfer function [2], which is in general difficult to know accurately. With this method, $\tilde{\imath}_{\mathrm{en}}$ can be obtained as:

$$\tilde{\imath}_{\mathrm{en}} = \left(\frac{2qI_{\mathrm{DC}}}{\left(\frac{\tilde{v}_{\mathrm{sn}}}{\tilde{v}_{\mathrm{dark}}}\right)^2 - 1} \right)^{1/2} \quad [\mathrm{A/Hz^{1/2}}], \tag{7}$$

where q is again the charge of an electron, $\tilde{v}_{\mathrm{sn}}$ and $\tilde{v}_{\mathrm{dark}}$ are the voltage noise densities at the output of the PR with and without illumination, respectively, and I_{DC} is the current produced by the photodiode under illumination.

Figure 5 presents $\tilde{\imath}_{\mathrm{en}}$ for a single channel of a GRACE-FO PRF (in cold redundancy). The requirement in this configuration is 5 $\mathrm{pA/Hz^{1/2}}$ at 16 MHz. The value obtained is around 3.5 $\mathrm{pA/Hz^{1/2}}$, fulfilling the requirement. The measurement was repeated for all channels of all PRFs obtaining similar results.

In May 2015, the GRACE-FO PR flight hardware was tested in a thermal vacuum chamber (TVAC) in order to verify correct operation in space conditions. The setup shown in Fig. 6 was used for that purpose. The full PR (PRFs and PRB) was placed inside the TVAC, together with infrared LEDs whose purpose was the simulation of beat notes on the PRFs. The optical power produced by each LED reaching the photodiode was in the order of 100 µW. The LEDs were amplitude-modulated from the outside using a frequency sweep from 4 to 16 MHz, which is the nominal GRACE-FO Doppler frequency range. Outside the tank, the phases of the PR signals from the different channels $\phi_X = \{\phi_{\mathrm{A}}, \phi_{\mathrm{B}}, \phi_{\mathrm{C}}, \phi_{\mathrm{D}}\}$ were measured against the reference signal from the LED driver source ϕ_{REF}. The TVAC temperature changed during the test with a nominal range of [-10,60] °C for the PRFs and [-15,55] °C for the PRB. The real temperature of the PRB, the most temperature sensitive element of the PR due to the AAF, was sensed during the test by

Optics EXPRESS

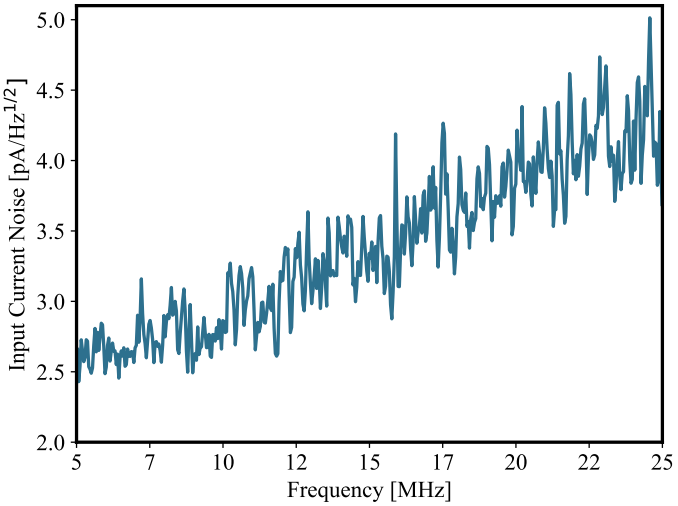

Fig. 5. Input noise density $\tilde{\imath}_{\mathrm{en}}$ for a single channel measured using cold redundancy (only one PRF). The requirement for GRACE-FO in this configuration is 5 pA/Hz$^{1/2}$ at 16 MHz. The value obtained is around 3.5 pA/Hz$^{1/2}$, fulfilling the requirement. The measurement was repeated for all channels of all PRFs obtaining similar results.

a PT1000 resistance temperature detector (RTD) inside the unit. Using this temperature and the phasemeter data, the temperature coefficients that define the thermal-induced phase noise in the PRs were experimentally measured.

A picture of all 3 PR flight models prior to the TVAC test can be seen in Fig. 7. The three PRBs are placed on the top base plate and the six PRFs (only 3 visible) on the lower base plate. The LEDs were mounted underneath the PRFs.

As mentioned in Section 2, the QPD used in the PR provides four different signals to simultaneously detect longitudinal displacements and angular misalignment between the two interfering beams. Since the 4 PR signals were tracked independently by the PM, the phase stability over temperature could be obtained for the main longitudinal measurand ϕ_{L} and also for all differential phase combinations needed to derive the angular misalignment (E.g. $\phi_{\mathrm{A}} - \phi_{\mathrm{B}}$). Figure 8 shows a diagram with the relation between the different quadrants and the longitudinal and differential phases.

Figure 9 shows a representative example of the longitudinal phase stability obtained during the TVAC test (from flight model #1). The longitudinal phase ϕ_{L} was recorded for a total of 61 PRB temperatures (between -6.4 °C and 63.2 °C) at each 1 KHz-frequency bin within the GRACE-FO Doppler frequency range. The plot on the left shows ϕ_{L} for the minimum and maximum temperatures. Since the results showed a mostly linear dependence of ϕ_{L} on temperature, a linear fit was performed to obtain the temperature coefficient ϕ_{LT} plotted on the right. There is an expected loss of phase over frequency due to the TIA and the AAF, increased by the low pass filtering from the meter-length cables used during the test. The maximum temperature coefficient ϕ_{LT} obtained (in absolute terms) is below -5 mrad/K at 16 MHz. This is not exactly the coefficient from the PR, since the LED source used has also a temperature dependency of about -2.5 mrad/K at 16 MHz, therefore with same sign. The LEDs were placed inside the tank and had a temperature profile similar to the PRFs. The value measured is nonetheless suitable as an upper limit for the longitudinal phase stability. Additionally, even if the configuration used

Optics EXPRESS

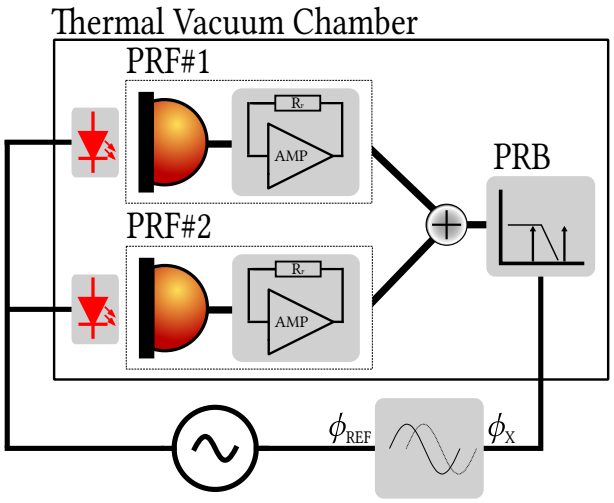

Fig. 6. Block diagram of the setup used during the TVAC test. The full PR (PRFs and PRB) was placed inside the TVAC, together with infrared LEDs for beat note simulation. The LEDs were amplitude-modulated using a frequency sweep from 4 to 16 MHz. The phases of the PR signals $\phi_X = \{\phi_A, \phi_B, \phi_C, \phi_D\}$ were measured against the reference signal from the LED driver source ϕ_{REF}. The TVAC temperature changed during the test with a nominal range of [-10,60] °C for the PRFs and [-15,55] °C for the PRB. The real temperature of the PRB was sensed by a PT1000 resistance temperature detector (RTD) inside the unit. Using this temperature and the phasemeter data, the temperature coefficient that defines the thermal-induced noise in the PR phase was experimentally measured.

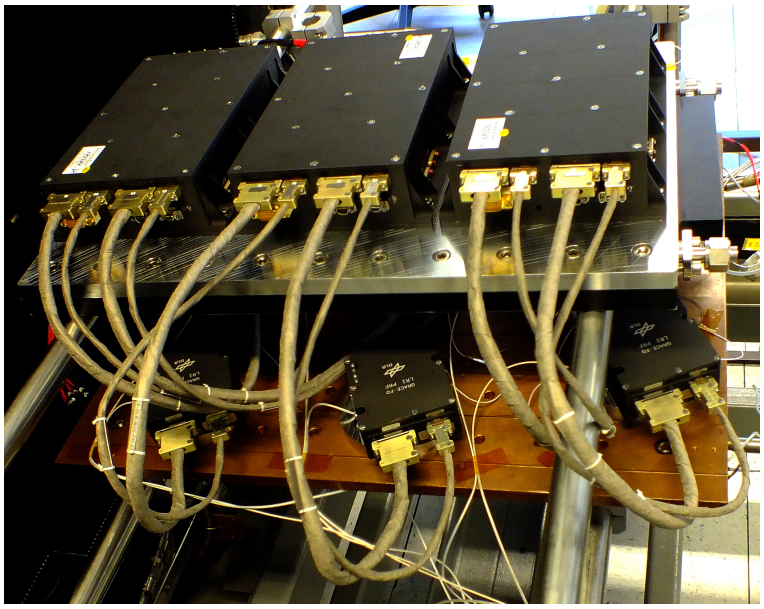

Fig. 7. A picture of all 3 PR flight models prior to the TVAC test. The three PRBs are placed on the top base plate and the six PRFs (only 3 visible) on the lower base plate. The LEDs were mounted underneath the PRFs.

Optics EXPRESS

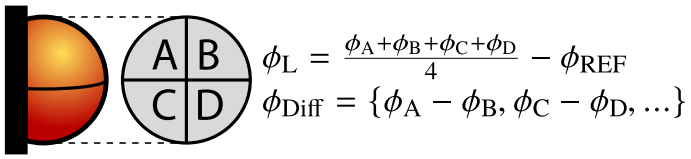

Fig. 8. Diagram with the relation between the different quadrants and the longitudinal and differential phases. The main longitudinal phase ϕ_L is an average of the 4 different channels measured against the reference phase ϕ_{REF}. The differential phase between the channels ϕ_{Diff} is needed to derive the angular misalignment between the interfered beams.

was hot redundant, the major contribution to ϕ_{LT} comes from the PRB, making the measured value suitable for noise budget calculations in cold redundancy (one PRF) and for comparison to the requirement (25 mrad/K).

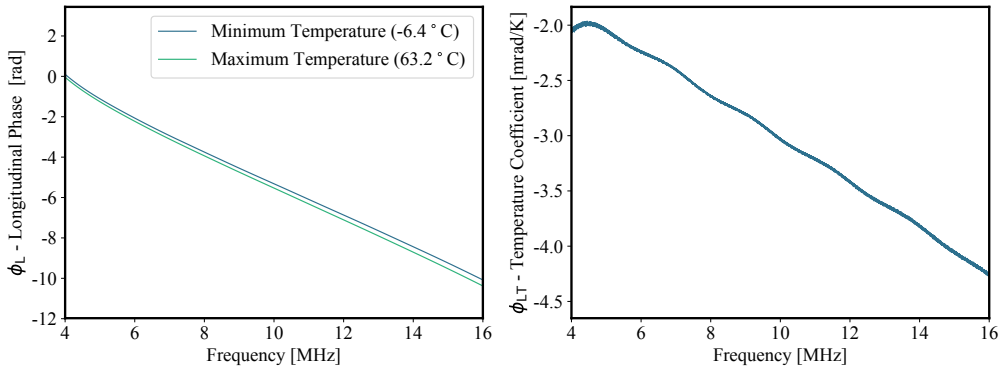

Fig. 9. Representative example of the longitudinal phase stability obtained during the TVAC test (from flight model #1). The longitudinal phase ϕ_L was recorded for a total of 61 PRB temperatures (between -6.4 °C and 63.2 °C) at each 1 KHz-frequency bin within the GRACE-FO Doppler frequency range. The plot on the left shows ϕ_L for the minimum and maximum temperatures. Since the results showed a mostly linear dependence of ϕ_L on temperature, a linear fit was performed to obtain the temperature coefficient ϕ_{LT} plotted on the right. The maximum ϕ_{LT} obtained (in absolute terms) is below -5 mrad/K at 16 MHz. This value is not exactly the coefficient from the PR, since the LED source used has also a temperature dependency of about -2.5 mrad/K at 16 MHz. The value measured is nonetheless suitable as an upper limit for the longitudinal phase stability. The requirement of 25 mrad/K is fulfilled.

Figure 10 shows a representative example of the differential phase stability obtained during the TVAC test ($\phi_A - \phi_D$ of PR flight model #1). In the same way as for ϕ_L, the differential phase ϕ_{Diff} is plotted on the left for the minimum and maximum PRB temperatures measured during the test. A mostly linear dependence of ϕ_{Diff} on temperature was observed. Therefore a linear fit provided again the temperature coefficient ϕ_{DiffT} plotted on the right. Since the differential phase does not require the use of a phase reference, the temperature coefficient of the LED does not affect the result. The maximum ϕ_{DiffT} obtained (in absolute terms) is about -100 µrad/K, 2 orders of magnitude below the 10 mrad/K requirement from GRACE-FO.

Optics EXPRESS

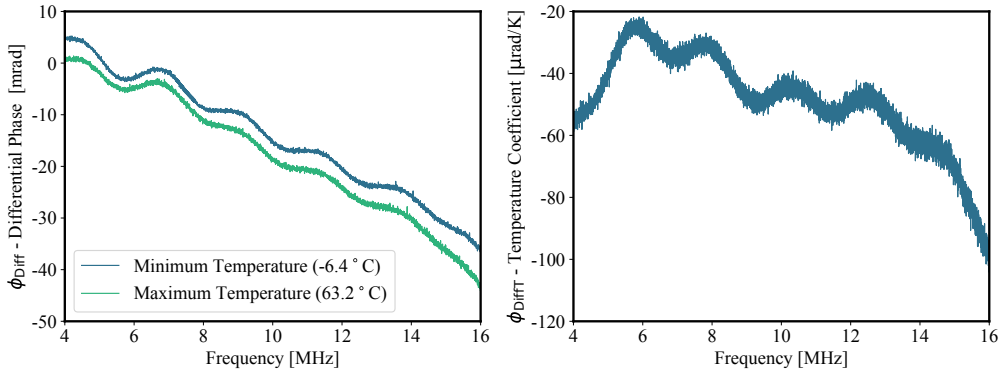

Fig. 10. Representative example of the differential phase stability ($\phi_A - \phi_D$ of PR flight model #1). The differential phase ϕ_{Diff} is plotted on the left for the minimum and maximum PRB temperatures measured during the test. A mostly linear dependence of ϕ_{Diff} on temperature was observed. Therefore a linear fit provided again the temperature coefficient ϕ_{DiffT} plotted on the right. Since the differential phase does not require the use of a phase reference, the temperature coefficient of the LED does not couple. The maximum temperature coefficient obtained in absolute terms is about -100 μrad/K, 2 orders of magnitude below the 10 mrad/K requirement from GRACE-FO.

5. Conclusion

We have analyzed in detail the main noise sources present in a PR used for intersatellite laser interferometry. A noise budget calculation using the PR requirements and expected interferometer parameters of the GRACE-FO mission indicates that the performance is shot-noise limited at 10^{-4} rad/Hz$^{1/2}$ down to 10^{-2} Hz, which is almost 4 orders of magnitude below the GRACE-FO LRI top level requirement ($\sim$ 0.5 rad/Hz$^{1/2}$). For lower frequencies however, the PR finite phase response noise dominates, mainly due to the $\tilde{f}_{\mathrm{Doppler}}$ contribution. This phase noise level at low frequencies is still compliant with the extended LRI top level requirement. For the LISA mission, the $\tilde{f}_{\mathrm{Doppler}}$ contribution is expected out-of-band (below 10^{-4} Hz). However, the finite phase response noise contribution due to $\tilde{f}_{\mathrm{laser}}$ could be a potential issue because of the more stringent noise budget of the mission [7]. This needs to be considered during the development and characterization of the LISA PR.

Results from the characterization of the GRACE-FO PR flight models have been presented as well. First, the electronic noise contribution $\tilde{\imath}_{\mathrm{en}}$ obtained was 3.5 pA/Hz$^{1/2}$ at 16 MHz for a single channel of the PR in cold redundancy. This fulfills the 5 pA/Hz$^{1/2}$ requirement for GRACE-FO but could suppose an excessive electronic noise contribution at the high frequencies in LISA, where shot-noise should also be dominating. For the LISA PR, designs based on ultra-low noise discrete transistors in combination with OpAmps are planed to be used to reduce $\tilde{\imath}_{\mathrm{en}}$ further. During the TVAC test of the GRACE-FO PR flight models, an upper limit for temperature coefficient of the longitudinal phase ϕ_{LT} was obtained. This was below -5 mrad/K at 16 MHz, fulfilling the 25 mrad/K requirement for the mission. In the same test, a maximum temperature coefficient (in absolute terms) for the differential phase ϕ_{DiffT} was derived as well. This coefficient of -100 µrad/K is two orders of magnitude below the 10 mrad/K requirement.

Funding

Bundesministerium für Bildung und Forschung (BMBF) (03F0654B); International Max Planck Research School on Gravitational Waves (IMPRS-GW).

Optics EXPRESS

Acknowledgments

The authors would like to thank the Deutsches Zentrum für Luft- und Raumfahrt (DLR) for the development of the GRACE-FO PR flight models, and Vitali Müller for the fruitful discussions about the GRACE satellites velocities and data provided.